This Accepted Manuscript has not been copyedited and formatted. The final version may differ from this version.

JNeurosci
THE JOURNAL OF NEUROSCIENCE

JNeurosci Accepted Manuscript

Research Articles: Systems/Circuits

A high-resolution in vivo atlas of the human brain's serotonin system

Vincent Beliveau[1,2], Melanie Ganz[1], Ling Feng[1], Brice Ozenne[1,3], Liselotte Højgaard[2,4], Patrick M. Fisher[1], Claus Svarer[1], Douglas N. Greve[5,6] and Gitte M. Knudsen[1,2]

[1]Neurobiology Research Unit and Center for Integrated Molecular Brain Imaging, Rigshospitalet, DK-2100 Copenhagen, Denmark

[2]Faculty of Health and Medical Sciences, Copenhagen University, DK-2100 Copenhagen, Denmark

[3]Department of Public Health, Section of Biostatistics, Copenhagen University, DK-2100 Copenhagen, Denmark

[4]PET and Cyclotron Unit, Copenhagen University Hospital, Rigshospitalet, DK-2100 Copenhagen, Denmark

[5]Athinoula A. Martinos Center for Biomedical Imaging, Department of Radiology, Massachusetts General Hospital, Boston, MA 02129, USA

[6]Harvard Medical School, Boston, MA 02115, USA

DOI: 10.1523/JNEUROSCI.2830-16.2016

Received: 8 September 2016

Revised: 8 November 2016

Accepted: 12 November 2016

Published: 17 November 2016

Author contributions: V.B., P.M.F., C.S., D.N.G., and G.M.K. designed research; V.B. and L.H. performed research; V.B., M.G., L.F., and B.O. analyzed data; V.B., M.G., L.F., B.O., L.H., P.M.F., C.S., D.N.G., and G.M.K. wrote the paper.

Conflict of Interest: V.B., M.G., L.F., P.M.F., C.S. and D.N.G. declare no competing financial interest. G.M.K. has been an invited lecturer at Pfizer A/S, worked as a consultant and received grants from H. Lundbeck A/S and is a stock holder of Novo Nordisk/Novozymes. Furthermore, she is on the board of directors of the BrainPrize and Elsass foundation and the advisory board of the Kristian Jebsen Foundation and has authored for FADL and served as editor for Elsevier (IJNP). L.H. is chairman of the board of the Danish National Research Foundation, and on the board of the Science advisory board of the Olav Thon Foundation and chairman of the Advisory Board of EU Horizon 2020, Health demographic change and wellbeing.

Collection of data included in the study was supported by the Lundbeck Foundation Center Cimbi (R90-A7722). V.B. was supported by the Danish Council for Independent Research - Medical Sciences (4183-00627) and the Research Council of Rigshospitalet (R84-A3300). M.G. was supported by the Carlsberg foundation (2013-01-0502) and National Institutes of Health (5R21EB018964-02). L.F. was supported by the European Union's Seventh Framework Programme (FP7/2007-2013) under grant agreement n° HEALTH-F2-2011-278850 (INMiND). D.N.G. research was supported by the NIH grant Multimodal Brain Imaging of Serotonin (5R21EB018964-02) and the MGH grant Shared Instrumentation Grant (S10RR023043). We thank The John and Birthe Meyer Foundation for providing the PET HRRT scanner.

Corresponding Author: Gitte M. Knudsen, MD, DMSc, Neurobiology Research Unit, Rigshospitalet, 9 Blegdamsvej, Section 6931, DK-2100 Copenhagen, Denmark, Phone: +45 3545 6720, E-mail: gmk@nru.dk

Cite as: J. Neurosci 2016; 10.1523/JNEUROSCI.2830-16.2016

Alerts: Sign up at www.jneurosci.org/cgi/alerts to receive customized email alerts when the fully formatted version of this article is published.

Accepted manuscripts are peer-reviewed but have not been through the copyediting, formatting, or proofreading process.

Copyright © 2016 the authors

JNeurosci Accepted Manuscript

A high-resolution in vivo atlas of the human brain's serotonin system

Vincent Beliveau[1,2], Melanie Ganz[1], Ling Feng[1], Brice Ozenne[1,3], Liselotte Højgaard[2,4], Patrick M. Fisher[1], Claus Svarer[1], Douglas N. Greve[5,6], Gitte M. Knudsen[1,2,*]

[1]Neurobiology Research Unit and Center for Integrated Molecular Brain Imaging, Rigshospitalet, DK-2100 Copenhagen, Denmark
[2]Faculty of Health and Medical Sciences, Copenhagen University, DK-2100 Copenhagen, Denmark
[3]Department of Public Health, Section of Biostatistics, Copenhagen University, DK-2100 Copenhagen, Denmark
[4]PET and Cyclotron Unit, Copenhagen University Hospital, Rigshospitalet, DK-2100 Copenhagen, Denmark
[5]Athinoula A. Martinos Center for Biomedical Imaging, Department of Radiology, Massachusetts General Hospital, Boston, MA 02129, USA
[6]Harvard Medical School, Boston, MA 02115, USA

*Corresponding Author
Gitte M. Knudsen, MD, DMSc
Neurobiology Research Unit
Rigshospitalet
9 Blegdamsvej, Section 6931
DK-2100 Copenhagen, Denmark
Phone: +45 3545 6720
E-mail: gmk@nru.dk

Pages: 20 Figures: 6 Tables: 2
Words: Abstract: 176 Introduction: 635 Discussion: 1291

Conflict of interest

V.B., M.G., L.F., P.M.F., C.S. and D.N.G. declare no competing financial interest. G.M.K. has been an invited lecturer at Pfizer A/S, worked as a consultant and received grants from H. Lundbeck A/S and is a stock holder of Novo Nordisk/Novozymes. Furthermore, she is on the board of directors of the BrainPrize and Elsass foundation and the advisory board of the Kristian Jebsen Foundation and has authored for FADL and served as editor for Elsevier (IJNP). L.H. is chairman of the board of the Danish National Research Foundation, and on the board of the Science advisory board of the Olav Thon Foundation and chairman of the Advisory Board of EU Horizon 2020, Health demographic change and wellbeing.

Acknowledgement

Collection of data included in the study was supported by the Lundbeck Foundation Center Cimbi (R90-A7722). V.B. was supported by the Danish Council for Independent Research - Medical Sciences (4183-00627) and the Research Council of Rigshospitalet (R84-A3300). M.G. was supported by the Carlsberg foundation (2013-01-0502) and National Institutes of Health (5R21EB018964-02). L.F. was supported by the European Union's Seventh Framework Programme (FP7/2007-2013) under grant agreement n° HEALTH-F2-2011-278850 (INMiND). D.N.G. research was supported by the NIH grant Multimodal Brain Imaging of Serotonin (5R21EB018964-02) and the MGH grant Shared Instrumentation Grant (S10RR023043). We thank The John and Birthe Meyer Foundation for providing the PET HRRT scanner.

JNeurosci Accepted Manuscript

Abstract

The serotonin (5-HT) system modulates many important brain functions and is critically involved in many neuropsychiatric disorders. We here present a high-resolution multi-dimensional *in vivo* atlas of four of the human brain's 5-HT receptors (5-HT_{1A}, 5-HT_{1B}, 5-HT_{2A}, and 5-HT_{4}) as well as of the 5-HT transporter (5-HTT). The atlas is created from molecular and structural high-resolution neuroimaging data consisting of Positron Emission Tomography (PET) and Magnetic Resonance Imaging (MRI) scans, acquired in a total of 210 healthy individuals. Comparison of the regional PET binding measures with postmortem human brain autoradiography outcomes showed a high correlation for the five 5-HT targets and this enabled us to transform the atlas to represent protein densities (pmol/ml). We also assessed the regional association between protein concentration and mRNA expression in the human brain by comparing the 5-HT density across the atlas to data from the Allen Human Brain atlas and identified receptor- and transporter specific associations which inform about the regional relation between the two measures. Together, these data provide unparalleled insight into the serotonin system of the human brain.

JNeurosci Accepted Manuscript

Significance Statement

We present a high-resolution PET and MR-based human brain atlas of important serotonin receptors and the transporter. The regional PET-derived binding measures correlate strongly with the corresponding autoradiography protein levels. The strong correlation enables the transformation of the PET-derived human brain atlas into a protein density map of the 5-HT system. Next, we compared the regional receptor/transporter protein densities to mRNA levels, and uncovered unique associations between protein expression and density at high detail. This new in vivo neuroimaging atlas of the 5-HT system does not only provide insight in the human brain's regional protein synthesis, transport and density, but also represents a valuable source of information for the neuroscience community as a comparative instrument to assess brain disorders.

JNeurosci Accepted Manuscript

Introduction

Serotonin (5-hydroxytryptamine, 5-HT) is a highly evolutionary conserved monoamine neurotransmitter that across species modulates multiple psycho-physiological functions. In the human brain, 5-HT is synthesized within the brainstems' raphe nuclei which have distributed efferent and afferent projections throughout the brain (Dorocic et al., 2014). The 5-HT system is highly diverse (Hannon and Hoyer, 2008); based on structural, transductional and operational features its receptors have been grouped into 7 families of receptors (5-HT_1 to 5-HT_7), including 14 known subtypes, and a transporter (5-HTT). Of the 14 receptors, there are 13 distinct G protein-coupled receptors and one ligand-gated ion channel receptor, the 5-HT_3. 5-HT is involved in myriad physiological functions such as cognition (Meneses, 1999), mood and social interaction (Young and Leyton, 2002), sexual behavior (Waldinger, 2015), feeding behavior (Magalhães et al., 2010), sleep-wake cycle (Portas et al., 2000) and thermoregulation (Cryan et al., 2000). Disturbances in the 5-HT system are also linked to many debilitating brain disorders such as major depression, anxiety, and schizophrenia as well as migraine and neurodegenerative disorders (Oades, 2010). The role of the individual receptors in the different functions and disorders is, however, only partially known. A prominent example is that even though the 5-HTT inhibitors (SSRIs) are the most frequently prescribed antidepressant drug class, the exact involvement of individual 5-HT receptors in mediating its clinical effects is still unclear. To study the role of the individual receptors in healthy individuals, in patients with brain disorders and in response to physiological or drug interventions, in vivo molecular brain imaging with positron emission tomography (PET) in conjunction with an appropriate radiotracer represents the state-of-the-art approach for quantifying the density and spatial distribution of brain receptors and transporters.

Brain atlases play a key role in neuroimaging research. Stereotactic atlases of magnetic resonance imaging (MRI) brain morphology such as the Talairach (Talairach and Tournoux, 1988) and the Montreal Neurological Institute (MNI) atlas (Evans et al., 1992) have become fundamental pillars for performing group analysis and anatomical segmentations such as the Automated

JNeurosci Accepted Manuscript

Anatomical Labeling atlas (Tzourio-Mazoyer et al., 2002) are commonly used to report results of regional outcomes of brain imaging data. A high-resolution human brain atlas of 5-HT receptors will represent a valuable tool for neuroimaging studies investigating the 5-HT system and disorders related to its dysfunction.

The distribution of 5-HT receptors in the human post-mortem brain has in the past been extensively described by autoradiography. However, autoradiography measurements, although quantitative, provide far less spatial information than a whole-brain atlas. With the development of well-validated radioligands for imaging the 5-HT system in vivo, it is now possible to image specific 5-HT receptor subtypes and the 5-HT transporter. Up to now, specific and validated PET radioligands for use in humans have been developed for the receptors 5-HT_{1A}R, 5-HT_{1B}R, 5-HT_{2A}R, 5-HT_{4}R and for 5-HTT (Paterson and Kornum, 2013). A radioligand for the 5-HT_{6} receptor has been validated in humans (Parker et al., 2012) but was not included here because it also has high affinity to the 5-HT_{2A} receptor (Parker et al., 2015).

We here present an MRI- and PET-based high-resolution atlas of the human brain 5-HT receptors 5-HT_{1A}R, 5-HT_{1B}R, 5-HT_{2A}R, 5-HT_{4}R and the 5-HTT, represented both in volume and on the cortical surface. The atlas was generated using a subset of the Center for Integrated Molecular and Brain Imaging's (Cimbi) extensive database (Knudsen et al., 2015), including 210 healthy volunteers aged between 18 and 45 years. Regional PET binding values were compared to corresponding post-mortem autoradiography data (Bonaventure et al., 2000; Varnäs et al., 2004) allowing us to validate our results and convert binding values into densities. Furthermore, regional densities were compared with mRNA levels from the Allen Human Brain Atlas (Hawrylycz et al., 2012; French and Paus, 2015) to confirm previous findings and gain novel insights into the localization of the receptor/transporter protein versus its expression.

Materials & Methods

Participants

JNeurosci Accepted Manuscript

All participants included in this study were healthy male and female controls from the Cimbi database (Knudsen et al., 2015); all data from this database is freely accessible. The data analysis was restricted to include individuals aged between 18 and 45 years. Participants were recruited by advertisement for different research protocols approved by the Ethics Committee of Copenhagen and Frederiksberg, Denmark. A total of 232 PET scans and corresponding structural MRI scans were acquired for 210 individual participants; 189 subjects had only 1 scan, 20 subjects had 2 scans and a single had 3 scans. Demographics details are presented in Table 1.

Positron Emission Tomography and Structural MRI

PET data was acquired in list-mode on a Siemens HRRT scanner operating in 3D-acquisition mode, with an approximate in-plane resolution of 2 mm (1.4 mm in the center of the field of view and 2.4 mm in cortex) (Olesen et al., 2009). PET frames were reconstructed using a 3D-OSEM-PSF algorithm (Comtat et al., 2008; Sureau et al., 2008). Scan time and frame length were designed according to the radiotracer characteristics. Dynamic PET frames were realigned using AIR 5.2.5 (Woods et al., 1992). See Table 2 for details on framing and realignment. T1 and T2-weighted structural MRI were acquired on four different Siemens scanners with standard parameters. All structural MRIs (T1 & T2) were unwarped offline using FreeSurfer's gradient_nonlin_unwarp v0.8 or online on the scanner (Jovicich et al., 2006). For further details on structural MRI acquisition parameters, see Knudsen et al. (2015).

Further processing was performed with FreeSurfer 5.3 (Fischl 2012, http://surfer.nmr.mgh.harvard.edu) using a surface and a volume stream. The individual cortical surfaces were reconstructed using the structural MRI corrected for gradient non-linearities. The pial surfaces were further refined using T2-weighted structural images and manually corrected where necessary. PET-MR coregistration was estimated using boundary-based registration (Greve and Fischl, 2009) between the time-weighted sum of the PET time-activity curves (TAC) and the structural MRI. Additionally, the transformation from individual MR space to normal MNI152 space was estimated with Combined Volume-Surface registration (Postelnicu et al., 2009) (CVS).

JNeurosci Accepted Manuscript

Regional TACs for the cortical regions were extracted by resampling the TACs to the cortical surface (Greve and Fischl, 2009) and taking the average within each of the 34 regions defined by the Desikan-Killiany cortical atlas (Desikan et al., 2006) automatically labeled by FreeSurfer. Similarly, regional TACs for 7 subcortical regions were obtained by resampling the TACs to an MR-based refined version of the automatic volume segmentation derived by FreeSurfer for each subjects as describe in Greve et al. (2016). Additionally, a segmentation of cerebellum including different lobules (e.g. vermis) were created using SUIT 2.7 (Diedrichsen, 2006) and SPM12 (http://www.fil.ion.ucl.ac.uk/spm). Gray matter cerebellar segmentations used as reference region were created by limiting the FS segmentation to the intersection with the cerebellum labeled by SUIT, excluding vermis; this has the effect of removing peripheral overlabeling sometimes present in the cerebellar segmentations.

Due to the high binding of [^{11}C]DASB and [^{11}C]CUMI-101 within dorsal and median raphe, these ROIs can be delineated directly on PET images. Raphe TACs were obtained by delineating the ROIs on the time-weighted summed TACs using anatomical landmarks from structural MRI according to the method described in Beliveau et al. (Beliveau et al., 2015) and extracting the average TACs within these regions. For the other tracers, raphe TACs were obtained by taking the average within normalized dorsal and median raphe templates. These templates were created by transferring the raphe ROIs previously derived to common space (MNI152) using CVS and taking the voxels with the highest overlap with a target volume of 150 mm^3 and 100 mm^3 for dorsal and median raphe, respectively. The delineations and templates were transferred back to PET space using CVS.

Subcortical voxel-wise TACs in common volume space (MNI152) were obtained using CVS. Cortical vertex-wise TACs in common surface space (fsaverage) were obtained using the cortical-surface alignment estimated by FreeSurfer (Fischl et al., 1999). Finally, cortical and subcortical TACs were respectively surface smoothed by 10mm and volume smoothed by 5mm full width half maximum.

JNeurosci Accepted Manuscript

Kinetic Modeling

For all radioligands modeling of the parametric and regional BP_{ND} was performed using the FS PET pipeline (Greve et al., 2013) with a Multilinear Reference Tissue Model 2 (MRTM2) (Ichise et al., 2003) using cerebellar gray matter, excluding vermis, as a reference region .The reference region washout rate (k_2') was computed using MRTM (Ichise et al., 1996); the high-binding TAC was obtained from a surface-weighted average of neocortical regions for [^{11}C]CUMI-101, [^{11}C]AZ10419369 and [^{11}C]Cimbi-36, and from a volume-weighted average of caudate and putamen for [^{11}C]SB207145 and of caudate, putamen and thalamus for [^{11}C]DASB. Parametric and regional BP_{ND} were thresholded between 0 and 10 (outliers were set to the corresponding threshold value) and average maps were created. For 5-HTT, the TAC of the median raphe was found to be irreversible within the scan time, hence the BP_{ND} for this region is not reported and it was disregarded from further analysis.

In Vivo Binding and Autoradiography

In order to compare our results to those of Varnäs et al. (2004) and Bonaventure et al. (2000), regional values were adapted. First, the autoradiography data from Varnäs et al. was averaged across layers for individual cortical regions and divisions of subcortical structures were averaged to generate larger identifiable structures. Then each region of the Desikan-Killiany cortical atlas (both left and right independently) as well as each subcortical region were grouped according to a set of regions common to the autoradiography data. Regional BP_{ND} values were then averaged within group using a volume/surface-weighting. Regions where no reasonable pairing could be made were disregarded. The association between BP_{ND} and autoradiography was estimated using a linear regression without intercept, as a null density is expected to yield null binding, and the estimated slopes were used to transform BP_{ND} into density values. Pearson's and Spearman's correlation coefficients were also computed for all associations. The Shapiro-Wilks test was used to assess the normality of the residuals and the null-hypothesis of normality was rejected for $p<0.1$; whenever the residuals did not pass the test, only the Spearman's correlation coefficient is reported. Densities in

JNeurosci Accepted Manuscript

203 units of pmol/g tissue were converted to pmol/ml using an approximate gray matter density of 1.045
204 g/ml (DiResta et al., 1991).

205 A linear mixed-effect model was used to investigate the global effect of age and gender on
206 the regional density for the five 5-HT targets. The model included age, gender and the interaction
207 between age and gender as a fixed effect. Region-specific random effects were used to model
208 regional-specific densities and subject-specific random effects to account for the correlation
209 between the regional measurements of a given individual. To handle different variability in 5-HT
210 density between regions, a separate variance parameter was estimated for each region. To
211 investigate a possible regional-specific effect of age or gender, a separate linear regression was
212 fitted to each region including age, gender and a possible interaction between age and gender as
213 covariates. In the global models, the p-values were adjusted for multiple comparison over tracers
214 (n=5) controlling the false discovery at 5% (Benjamini and Hochberg, 1995). Similarly, regional
215 models were corrected for multiple comparison over regions (n=42). For the entire analysis, the
216 significance threshold was fixed at $p<0.05$. Regional densities were averaged for left and right
217 hemispheres.

218 The BP_{ND} of small volume of interest surrounded by low binding tissue can be drastically
219 underestimated due to partial volume effects. As previously described (Savli et al., 2012), this is
220 particularly pronounced in the raphe nuclei for the 5-HTT and 5-HT_{1A}R as there is high binding for
221 the corresponding radioligand in this region, but much lower levels in to neighboring white matter
222 tissue of the brainstem. Accordingly, the raphe nuclei density values reported here should be
223 interpreted with caution and, although they are depicted in Figure 1 and 5, this region was excluded
224 from any quantitative analysis for the 5-HTT and the 5-HT_{1A}R. Similarly, the 5-HTT BP_{ND}
225 distribution within globus pallidus was found to be highly heterogeneous due to partial volume
226 effect from the caudate, hence this region was also excluded from quantitative analysis for the 5-
227 HTT.

228 **In Vivo Binding and mRNA Levels**

JNeurosci Accepted Manuscript

Regional binding values were compared to 5-HT receptors and transporter mRNA normalized expression values from the Allen Human Brain Atlas (Hawrylycz et al., 2012). The atlas contains probe information from 6 human brains. Each probe is associated with mRNA levels (log2 intensity) for all genes sequenced, an anatomical label and coordinates in the MNI152 space, as well as many other parameters. For more details on the material and methods for the Allen Human Brain Atlas, see the Microarray Survey Technical White papers available at (http://help.brain-map.org/display/humanbrain/Documentation). mRNA expression values for regions of the Desikan-Killiany cortical atlas were obtained from the work of French and Paus (2015). Each probe of the Allen Human Brain Atlas was paired to a cortical region using its coordinates in the MNI152 space and regional expression values were obtained by averaging expression values across probes, and then by taking the median per regions and finally taking the median across subjects. We used the same approach to obtain subcortical expression values, however probes were paired to subcortical regions directly by their anatomical label rather than using their coordinates to identify corresponding regions. Both binding values and mRNA values were averaged between left and right hemispheres. As above, the association between binding and mRNA was estimated using a linear regression and Pearson's and Spearman's correlation coefficients were also computed for all association. Dorsal raphe was excluded from the regression for 5-HTT and 5-HT_{1A}R and the regression was performed for cortical regions only for the 5-HT_{2A}R. For 5-HT_{1B}R and 5-HT_{2A}R subcortical regions exhibited patterns distinct from the cortical regions, hence the analysis was stratified between cortical and subcortical regions for these two targets.

Results

In Vivo Molecular Imaging and Autoradiography

Brain regional BP_{ND} values were compared to the corresponding receptor density measurements from post-mortem autoradiography data from Varnäs et al. (2004) and Bonaventure et al. (2000) (for 5-HT_4R). Figure 1 (A-E) shows the relation between autoradiography receptor/transporter B_{max} from the two studies and PET measures of BP_{ND} from the Cimbi database.

JNeurosci Accepted Manuscript

For all five targets, we found good to excellent associations between BP_{ND} and B_{max}, with Pearson's correlation coefficients ranging from 0.88 to 0.97 and Spearman's correlation coefficients ranging from 0.72 to 0.97. For 5-HTT, the residuals for 5-HTT did not pass the Shapiro-Wilks test for normality, hence the Pearson's correlation is not reported for that association. The slope estimates of the regression were used to transform the BP_{ND} atlases into B_{max} atlases (Figure 2 and 3), allowing for a direct comparison across targets. The regional densities are presented in Figure 4. No global or regional significant effect of age, gender or their interaction was found.

Receptor Density and mRNA

The associations between in vivo receptor density, obtained by converting BP_{ND} into densities, and mRNA levels are shown in Figure 5. For the 5-HT_{1A}R, we found excellent correlation between the protein densities and mRNA levels, with Pearson's and Spearman's correlation coefficients of 0.94 and of 0.94, respectively. For 5-HT_4, the residuals did not pass the Shapiro-Wilks test for normality, but we found a moderate Spearman's correlation coefficient of 0.50. The 5-HT_{1B}R and 5-HT_{2A}R showed a distinctly different pattern compared to other targets, with good Pearson's correlation coefficients (0.66 and 0.60, respectively) and weak to moderate Spearman's correlation coefficients (0.28 and 0.46) in cortical regions, but there was no statistically significant correlation in subcortical regions.

DISCUSSION

We here present the first high-resolution PET- and MR-based in vivo human brain atlas of four 5-HT receptors and the transporter. The atlas highlights key features of the 5-HT targets; their spatial distribution and abundance relative to each other. As we identified high correlations with post-mortem autoradiography receptor measurements, the atlas could be calibrated to represent absolute receptor or transporter densities, thus making the atlas independent of the PET methodology in terms of choice of radiotracer and modeling approach. Access to such a high-resolution atlas of the 5-HT system enables scientists not only to evaluate the absolute densities of the individual targets, but also the relative abundance of protein, and in any brain region of interest.

JNeurosci Accepted Manuscript

A few caveats with this approach deserve, however, to be mentioned here. Whereas autoradiography provides a measurement of the target density, PET returns an outcome measure that is proportional to the density of the target available for radioligand binding, and the measure most notably depends on the in vivo radioligand affinity to the target. However, since the occupancy of endogenous 5-HT is low for most targets (Paterson et al., 2010) it is unlikely that individual differences in endogenous 5-HT (and thereby in vivo affinity) would incur any bias.

Although PET imaging offers unique sensitivity and specificity, the intrinsic image resolution of PET is lower than for MRI. A prior brain 5-HT atlas has been reported based on PET scanners with a resolution of 4.4 mm and was generated independent of anatomical MRI (Savli et al., 2012). Leveraging high-resolution structural MRI (~1 mm resolution) in combination with molecular images acquired with a high-resolution PET scanner with a resolution of 2 mm allows for precise segmentation of brain regions and accurate inter-subject normalization. The surface-based approach used in this work has also been shown to lead to a reduction in bias and variance of PET-derived measurements (Greve et al., 2013). A main advantage of the surface-based method is to diminish partial volume effects introduced by smoothing in the volume; smoothing on the surface drastically reduces the blurring of neighboring tissues with cortical gray matter as well as blurring across adjacent gyri (Jr et al., 2006). Nevertheless, we still see subtle signs suggestive of partial volume effects, e.g., bands of lower binding along the medial wall, see Figure 6. Although a partial volume corrected atlas could be generated, we chose not to do so because methods for partial volume corrections come with their own set of limitations (Harri et al., 2007) and can lead to different results depending on the algorithm used (Greve et al., 2016).

Although [^{11}C]Cimbi-36 has been shown to have some affinity for 5-HT$_{2C}$, these receptors are mostly limited to the choroid plexus and the hippocampus. Furthermore, binding measures for [^{11}C]Cimbi-36 have been shown to be very strongly correlated to those of the 5-HT$_{2A}$ antagonist radiotracer [^{18}F]Altanserin (Ettrup et al., 2016). Hence, any bias caused by the contribution of 5-HT$_{2C}$ receptors is expected to have minimal impact on the results presented here.

JNeurosci Accepted Manuscript

306 We compared our in vivo imaging atlases to meticulous autoradiography studies of the
307 relevant 5-HT targets in postmortem human brain slices (Bonaventure et al., 2000; Varnäs et al.,
308 2004). The postmortem brains in Varnäs et al. (2004) and Bonaventure et al. (2000) were retrieved
309 from individuals older than those included in our study, with respective mean age of 58 and 55
310 versus 26 years in our cohort. Thus, the atlas densities represent those that can be observed in
311 individuals matching the mean age of the population in the autoradiography studies. Within the
312 current cohort, we did not observe any significant effect of age or gender within our data, most
313 likely because of the limited age range of the subjects. Whereas some 5-HT targets, such as 5-
314 HT_{1B}R and 5-HT_{2A}R, are relatively independent of age others, have been shown to have a
315 pronounced age-dependent decline and/or sex-differences (Moses-kolko et al., 2011; Nord et al.,
316 2014). Hence, minor data adjustments may be necessary when relating these atlases to specific
317 research questions.

318 For all the serotonergic targets, except for the 5-HT_{1A}R (Rizzo et al., 2014), we provide
319 novel information about the relationship between in vivo molecular imaging in humans and the
320 associated mRNA levels assessed in postmortem human brain tissue. The relation between the
321 cerebral 5-HT target densities and their corresponding mRNA levels is of interest as mRNA levels
322 often do not correspond to their protein levels because protein concentrations depend on the relative
323 rates of transcription, mRNA decay, translation, and protein degradation (Vogel et al., 2010).
324 Relating the two measures in brain space generates important information about the gene-protein
325 translation. A high spatial correspondence between the two measures suggests that the protein is
326 located on or at least close to the cell body where the protein synthesis takes place. We found no
327 significant association between 5-HTT mRNA and 5-HTT density although as expected, both were
328 high in the dorsal raphe (Figure 5, A). This is consistent with the exclusively presynaptic
329 localization of 5-HTT and hence primary mRNA localization within raphe nuclei (Hoffman et al.,
330 1998) and 5-HTT protein being located on terminal projections distant from 5-HT neurons (Zhou et
331 al., 1998). The 5-HTT mRNA levels were overall low, both relative to the mRNA of other targets

JNeurosci Accepted Manuscript

and to the 5-HTT protein density. Consistent with Rizzo et al. (2014), we find a very strong association between 5-HT_{1A}R mRNA and 5-HT_{1A}R protein density as determined with in vivo molecular neuroimaging (Figure 5, B). Rizzo and colleagues ascribed the tight correlation to a more general feature of the serotonergic system but here we show that several other serotonergic targets show profound regional differences. We found a fair association between neocortical 5-HT_{1B}R mRNA and 5-HT_{1B}R density (Figure 5, C) but the subcortical regions did not conform to this association. As for the latter, our findings are consistent with a previous postmortem human brain study where proportionally higher levels of 5-HT_{1B}R mRNA than protein were found particularly in the ventral striatum, whereas the pallidum which is the brain region with the highest 5-HT_{1B}R density had low mRNA levels (Varnäs et al., 2005). This supports the observation in rodents that 5-HT_{1B}R in pallidum are localized in nerve terminals from striatal projections (Boschert et al., 1994), that are of GABAergic origin (Ghavami et al., 1999). To the best of our knowledge, existing literature does not provide evidence about the relative densities of 5-HT_{1B}R autoreceptors and heteroreceptors in different brain regions but due to the specific pattern observed here, we speculate that the 5-HT_{1B}R heteroreceptors may be relatively more abundant in subcortical regions. An interesting pattern of 5-HT_{2A}R mRNA versus 5-HT_{2A}R density emerged: whereas the neocortical brain regions showed a good, linear correlation, there was no association between the two measures in subcortical brain regions (Figure 5, D) and the neocortical and subcortical regions fall in two separate clusters on the graph. The pattern is in agreement with observations in the macaque monkey brain (López-Giménez et al., 2001) and suggests that the regulation and role of the 5-HT_{2A}R markedly differs between neocortical and subcortical brain regions, possibly because the 5-HT_{2A}R in neocortex are located in the apical part of pyramidal neurons (Jakab and Goldman-Rakic, 2000). In addition, the 5-HT_{2A}R mRNA levels are almost twice as high compared to the other investigated targets. We speculate that high mRNA levels enable the system to quickly regulate synaptic 5-HT_{2A}R levels, consistent with the ligand-induced endocytosis and recycling of 5-HT_{2A}R (Raote et al., 2013). We observed a moderate correlation association between 5-HT_4R mRNA and

JNeurosci Accepted Manuscript

358 5-HT_4R protein density (Figure 5, E). This finding is consistent with data obtained in human , where
359 5-HT_4R mRNA levels and densities where high in caudate, putamen, accumbens and the
360 hippocampus formation, and were both relatively lower in other brain regions.

361 **Conclusion**

362 We here present a comprehensive PET- and MR-based high-resolution brain atlas of the
363 serotonin system. By combining the *in vivo* atlases with postmortem autoradiography measurements,
364 we calibrated the individual atlas to represent quantitative protein levels in terms of pmol/ml.
365 Furthermore, we describe the relation between regional serotonergic target densities and their
366 mRNA levels, some for the first time in humans. The approach is generally applicable for any
367 molecular target that can be visualized in vivo by PET. Such publicly available in vivo human brain
368 atlases will serve as an important resource for neuroscience.
369

JNeurosci Accepted Manuscript

REFERENCES

Beliveau V, Svarer C, Frokjaer VG, Knudsen GM, Greve DN, Fisher PM (2015) Functional connectivity of the dorsal and median raphe nuclei at rest. Neuroimage 116:187–195.

Benjamini Y, Hochberg Y (1995) Controlling the false discovery rate: a practical and powerful approach to multiple testing. J R Stat Soc Ser B 57:289–300.

Bonaventure P, Hall H, Gommeren W, Cras P, Langlois X, Jurzak M, Leysen JE (2000) Mapping of serotonin 5-HT(4) receptor mRNA and ligand binding sites in the post-mortem human brain. Synapse 36:35–46.

Boschert U, Amara DA, Segu L, Hen R (1994) The mouse 5-hydroxytryptamine1B receptor is localized predominantly on axon terminals. Neuroscience 58:167–182.

Comtat C, Sureau FC, Sibomana M, Hong IK, Sjoholm N, Trebossen R (2008) Image based resolution modeling for the HRRT OSEM reconstructions software. In: 2008 IEEE Nuclear Science Symposium Conference Record, pp 4120–4123. IEEE.

Cryan JF, Harkin A, Naughton M, Kelly JP, Leonard BE (2000) Characterization of D - fenfluramine-induced hypothermia: evidence for multiple sites of action. Eur J Pharmacol 390:275–285.

Desikan RS, Ségonne F, Fischl B, Quinn BT, Dickerson BC, Blacker D, Buckner RL, Dale AM, Maguire RP, Hyman BT, Albert MS, Killiany RJ (2006) An automated labeling system for subdividing the human cerebral cortex on MRI scans into gyral based regions of interest. Neuroimage 31:968–980.

Diedrichsen JJ (2006) A spatially unbiased atlas template of the human cerebellum. Neuroimage 33:127–138.

DiResta GR, Lee J, Arbit E (1991) Measurement of brain tissue specific gravity using pycnometry. J Neurosci Methods 39:245–251.

Dorocic IP, Fürth D, Xuan Y, Johansson Y, Pozzi L, Silberberg G, Carlén M, Meletis K (2014) A Whole-Brain Atlas of Inputs to Serotonergic Neurons of the Dorsal and Median Raphe Nuclei. Neuron 83:663–678.

Ettrup A, Svarer C, McMahon B, da Cunha-Bang S, Lehel S, Møller K, Dyssegaard A, Ganz M, Beliveau V, Jørgensen LM, Gillings N, Knudsen GM (2016) Serotonin 2A receptor agonist binding in the human brain with [(11)C]Cimbi-36: Test-retest reproducibility and head-to-head comparison with the antagonist [(18)F]altanserin. Neuroimage 34:1188–1196.

Evans AC, Collins DL, Milner B (1992) An MRI- Based Stereotactic Atlas from 250 Young Normal Subjects. Soc Neurosci Abstr 18:408.

Fischl B (2012) FreeSurfer. Neuroimage 62:774–781.

Fischl B, Sereno MI, Tootell RBH, Dale AM (1999) High-resolution intersubject averaging and a coordinate system for the cortical surface. Hum Brain Mapp 8:272–284.

French L, Paus T (2015) A FreeSurfer view of the cortical transcriptome generated from the Allen Human Brain Atlas. Front Neurosci 9:1–5.

Ghavami a, Stark KL, Jareb M, Ramboz S, Ségu L, Hen R (1999) Differential addressing of 5-HT1A and 5-HT1B receptors in epithelial cells and neurons. J Cell Sci 112 Pt 6:967–976.

Greve DN, Fischl B (2009) Accurate and robust brain image alignment using boundary-based registration. Neuroimage 48:63–72.

Greve DN, Salat DH, Bowen SL, Izquierdo-Garcia D, Schultz AP, Catana C, Becker JA, Svarer C, Knudsen G, Sperling RA, Johnson KA (2016) Different partial volume correction methods lead to different conclusions: An 18F-FDG PET Study of aging. Neuroimage 132:334–343.

Greve DN, Svarer C, Fisher PM, Feng L, Hansen AE, Baare W, Rosen B, Fischl B, Knudsen GM (2013) Cortical surface-based analysis reduces bias and variance in kinetic modeling of brain PET data. Neuroimage 92C:225–236.

Hannon J, Hoyer D (2008) Molecular biology of 5-HT receptors. Behav Brain Res 195:198–213.

Harri M, Mika T, Jussi H, Nevalainen OS, Jarmo H (2007) Evaluation of partial volume effect correction methods for brain positron emission tomography: Quantification and reproducibility.

JNeurosci Accepted Manuscript

421 J Med Phys 32:108–117.
422 Hawrylycz MJ et al. (2012) An anatomically comprehensive atlas of the adult human brain
423 transcriptome. Nature 489:391–399.
424 Hoffman BJ, Hansson SR, Mezey E, Palkovits M (1998) Localization and dynamic regulation of
425 biogenic amine transporters in the mammalian central nervous system. Front Neuroendocrinol
426 19:187–231.
427 Ichise M, Ballinger J, Golan H (1996) Noninvasive quantification of dopamine D2 receptors with
428 iodine-123-IBF SPECT. J Nucl Med 37:513–520.
429 Ichise M, Liow J, Lu J, Takano A (2003) Reference Tissue Parametric Imaging Methods:
430 Application to [11C] DASB Positron Emission Tomography Studies of the Serotonin
431 Transporter in. J Cereb blood flow Metab 23:1096–1112.
432 Jakab RL, Goldman-Rakic PS (2000) Segregation of serotonin 5-HT2A and 5-HT3 receptors in
433 inhibitory circuits of the primate cerebral cortex. J Comp Neurol 417:337–348.
434 Jovicich J, Czanner S, Greve D, Haley E, van der Kouwe A, Gollub R, Kennedy D, Schmitt F,
435 Brown G, Macfall J, Fischl B, Dale A (2006) Reliability in multi-site structural MRI studies:
436 effects of gradient non-linearity correction on phantom and human data. Neuroimage 30:436–
437 443.
438 Jr DH, Saygin A, Sereno M, Hagler D (2006) Smoothing and cluster thresholding for cortical
439 surface-based group analysis of fMRI data. Neuroimage 33:1093–1103.
440 Knudsen GM et al. (2015) The Center for Integrated Molecular Brain Imaging (Cimbi) Database.
441 Neuroimage:1–7.
442 López-Giménez J, Vilaro TM, Palacios JM, Mengod G (2001) Mapping of 5-HT2A receptors and
443 their mRNA in monkey brain: [3H]MDL100,907 autoradiography and in situ hybridization
444 studies. J Comp Neurol 429:571–589.
445 Magalhães CP, de Freitas MFL, Nogueira MI, Campina RCDF, Takase LF, de Souza SL, de Castro
446 RM (2010) Modulatory role of serotonin on feeding behavior. Nutr Neurosci 13:246–255.
447 Meneses A (1999) 5-HT system and cognition. Neurosci Biobehav Rev 23:1111–1125.
448 Moses-kolko EL, Price JC, Shah N, Berga S, Sereika SM, Fisher PM, Coleman R, Becker C, Mason
449 NS, Loucks T, Meltzer CC (2011) Age , Sex , and Reproductive Hormone Effects on Brain
450 Serotonin-1A and Serotonin-2A Receptor Binding in a Healthy Population.
451 Neuropsychopharmacology 36:2729–2740.
452 Nord M, Cselenyi Z, Forsberg A, Rosenqvist G, Tiger M, Lundberg J, Varrone A, Farde L (2014)
453 Distinct regional age effects on [11C]AZ10419369 binding to 5-HT1B receptors in the human
454 brain. Neuroimage 103:303–308.
455 Oades RD (2010) Handbook of the Behavioral Neurobiology of Serotonin.
456 Olesen OV, Sibomana M, Keller SH, Andersen F, Jensen J, Holm S, Svarer C, Højgaard L (2009)
457 Spatial resolution of the HRRT PET scanner using 3D-OSEM PSF reconstruction. IEEE Nucl
458 Sci Symp Conf Rec:3789–3790.
459 Parker C a., Gunn RN, Rabiner E a., Slifstein M, Comley R, Salinas C, Johnson CN, Jakobsen S,
460 Houle S, Laruelle M, Cunningham VJ, Martarello L (2012) Radiosynthesis and
461 Characterization of 11C-GSK215083 as a PET Radioligand for the 5-HT6 Receptor. J Nucl
462 Med 53:295–303.
463 Parker CA, Rabiner EA, Gunn R, Searle G, Martarello L, Comley R, Davy M, Wilson AA, Houle S,
464 Mizrahi R, Laruelle M, Cunningham VJ (2015) Human kinetic modelling of the 5-HT6 PET
465 radioligand, 11C-GSK215083, and its utility for determining occupancy at both 5HT6 and
466 5HT2A receptors by SB742457 as a potential therapeutic mechanism of action in Alzheimer's
467 disease. J Nucl Med 56:1901–1909.
468 Paterson L, Kornum B (2013) 5-HT radioligands for human brain imaging with PET and SPECT.
469 Med Res Rev 33:54–111.
470 Paterson LM, Tyacke RJ, Nutt DJ, Knudsen GM (2010) Measuring endogenous 5-HT release by
471 emission tomography: promises and pitfalls. J Cereb Blood Flow Metab 30:1682–1706.
472 Portas CM, Bjorvatn B, Ursin R (2000) Serotonin and the sleep/wake cycle : special emphasis on

JNeurosci Accepted Manuscript

473 microdialysis studies. Prog Neurobiol 60:12–35.
474 Postelnicu G, Zollei L, Fischl B (2009) Combined volumetric and surface registration. Med
475 Imaging, IEEE Trans 28:508–522.
476 Raote I, Bhattacharyya S, Panicker MM (2013) Functional Selectivity in Serotonin Receptor 2A (5-
477 HT2A) Endocytosis, Recycling, and Phosphorylation. Mol Pharmacol 83:42–50.
478 Rizzo G, Veronese M, Heckemann RA, Selvaraj S, Howes OD, Hammers A, Turkheimer FE,
479 Bertoldo A (2014) The predictive power of brain mRNA mappings for in vivo protein density:
480 a positron emission tomography correlation study. J Cereb Blood Flow Metab 34:827–835.
481 Savli M, Bauer A, Mitterhauser M, Ding Y (2012) Normative database of the serotonergic system in
482 healthy subjects using multi-tracer PET. Neuroimage 63:447–459.
483 Sureau FC, Reader AJ, Comtat C, Leroy C, Ribeiro M-J, Buvat I, Trébossen R (2008) Impact of
484 image-space resolution modeling for studies with the high-resolution research tomograph. J
485 Nucl Med 49:1000–1008.
486 Talairach J, Tournoux P (1988) Co-planar stereotaxic atlas of the human brain: 3-dimensional
487 proportional system: an approach to cerebral imaging.
488 Tzourio-Mazoyer N, Landeau B, Papathanassiou D, Crivello F, Etard O, Delcroix N, Mazoyer B,
489 Joliot M (2002) Automated anatomical labeling of activations in SPM using a macroscopic
490 anatomical parcellation of the MNI MRI single-subject brain. Neuroimage 15:273–289.
491 Varnäs K, Halldin C, Hall H (2004) Autoradiographic distribution of serotonin transporters and
492 receptor subtypes in human brain. Hum Brain Mapp 22:246–260.
493 Varnäs K, Hurd YL, Hall H (2005) Regional expression of 5-HT1B receptor mRNA in the human
494 brain. Synapse 56:21–28.
495 Vogel C, Abreu R de S, Ko D, Le S-YY, Shapiro BA, Burns SC, Sandhu D, Boutz DR, Marcotte
496 EM, Penalva LO (2010) Sequence signatures and mRNA concentration can explain two-thirds
497 of protein abundance variation in a human cell line. TL - 6. Mol Syst Biol 6:400.
498 Waldinger MD (2015) Psychiatric disorders and sexual dysfunction., 1st ed. Elsevier B.V.
499 Woods RP, Cherry SR, Mazziotta JC (1992) Rapid automated algorithm for aligning and reslicing
500 PET images. J Comput Assist Tomogr 16:620–633.
501 Young S, Leyton M (2002) The role of serotonin in human mood and social interaction: insight
502 from altered tryptophan levels. Pharmacol Biochem Behav 71:857–865.
503 Zhou FC, Tao-Cheng JH, Segu L, Patel T, Wang Y (1998) Serotonin transporters are located on the
504 axons beyond the synaptic junctions: anatomical and functional evidence. Brain Res 805:241–
505 254.
506
507

JNeurosci Accepted Manuscript

FIGURES AND TABLE LEGENDS

Figure 1. Regional BP_{ND} and B_{max} values for the five 5-HT targets. The regions in the PET image space were combined to match the regions used by Varnäs et al. (2004) and Bonaventure et al. (2000) in their autoradiography measurement. The regressions (fixed through 0.0) are shown as black, dashed lines and the Pearson's (R) and Spearman's (S) correlation coefficients are reported; ** indicate $p<0.001$. Dorsal raphe, median raphe and globus pallidus for 5-HTT and dorsal raphe for 5-HT_{1A}R were excluded from the regressions and marked with + on the figure, see the Material & Methods section.

Figure 2. Average density (B_{max}) maps for five 5-HT targets on the common FreeSurfer surface (left hemisphere; lateral view, upper and medial view, lower). Color scaling was individually adjusted in order to highlight features of the distributions.

Figure 3. Average density (B_{max}) maps for the five 5-HT targets in the common MNI152 space (coronal, upper, z=8mm and sagittal, lower, x=-3mm). Color scaling was individually adjusted to highlight features of the distributions.

Figure 4. Density values (B_{max}) of the five 5-HT targets in FreeSurfer defined brain regions. Median raphe is not reported for 5-HTT due the irreversible kinetic of the TACs, see also the Material & Methods section.

Figure 5. Regional density values (B_{max}) and mRNA levels for the five 5-HT targets. Subcortical data is shown in color and cortical data is shown in black. The regression lines are shown as black dashed lines and the Pearson's (R) and Spearman's (S) correlation coefficients are reported; * and ** indicate $p<0.01$ and $p<0.001$, respectively. In panel C and D, a line was fitted to cortical regions (black) only. Dorsal raphe, median raphe and globus pallidus for 5-HTT and dorsal raphe for 5-HT_{1A}R were excluded from the regressions and marked with + on the figure, see also the Material & Methods section.

Figure 6. Average density (B_{max}) maps for five 5-HT targets on the inflated common FreeSurfer surface (left hemisphere; lateral view, upper and medial view, lower).

Table 1. Demographics of the healthy individuals.

Table 2. PET scanning and realignement parameters.

JNeurosci Accepted Manuscript

TABLES

Table 1. Demographics of the healthy individuals.

Receptor/transporter	5-HTT	5-HT_{1A}R	5-HT_{1B}R	5-HT_{2A}R	5-HT_4R
Radioligand	[^{11}C]DASB	[^{11}C]CUMI-101	[^{11}C]AZ10419369	[^{11}C]Cimbi-36	[^{11}C]SB207145
N	100	8	36	29	59
Gender (M/F)	29/71	3/5	24/12	15/14	41/18
Age (mean±sd)	25.1±5.8	28.4±8.8	27.8±6.9	22.6±2.7	25.9±5.3
BMI (kg/m^2) (mean±sd)	23.2±2.9	22.7±2.6	24.9±4.3	23.4±2.4	23.5±3.3
Injected dose (MBq) (mean±sd)	586.0±32.2	510.5±149.1	585.4±37.4	510.4±109.7	577.1±70.9
Injected Mass (μg) (mean±sd)	1.9±2.2	2.0±1.5	1.2±1.0	0.8±0.5	1.1±0.7

Table 2. PET scanning and realignement parameters.

Radioligand	[^{11}C]DASB	[^{11}C]CUMI-101	[^{11}C]AZ10419369	[^{11}C]Cimbi-36	[^{11}C]SB207145
Scan time (min)	90	120	90	120	120
Frame lengths (number x sec)	6x10, 3x20, 6x30, 5x60, 5x120, 8x300, 3x600	6x5, 10x15, 4x30, 5x120, 5x300, 8x600	6x10, 6x20, 6x60, 8x120, 19x300	6x10, 6x20, 6x60, 8x120, 19x300	6x5, 10x15, 4x30, 5x120, 5x300, 8x600
Realigned frames (first:last)	10:36	10:38	13:45	13:45	10:38
Reference frame	26	26	27	27	26

JNeurosci Accepted Manuscript

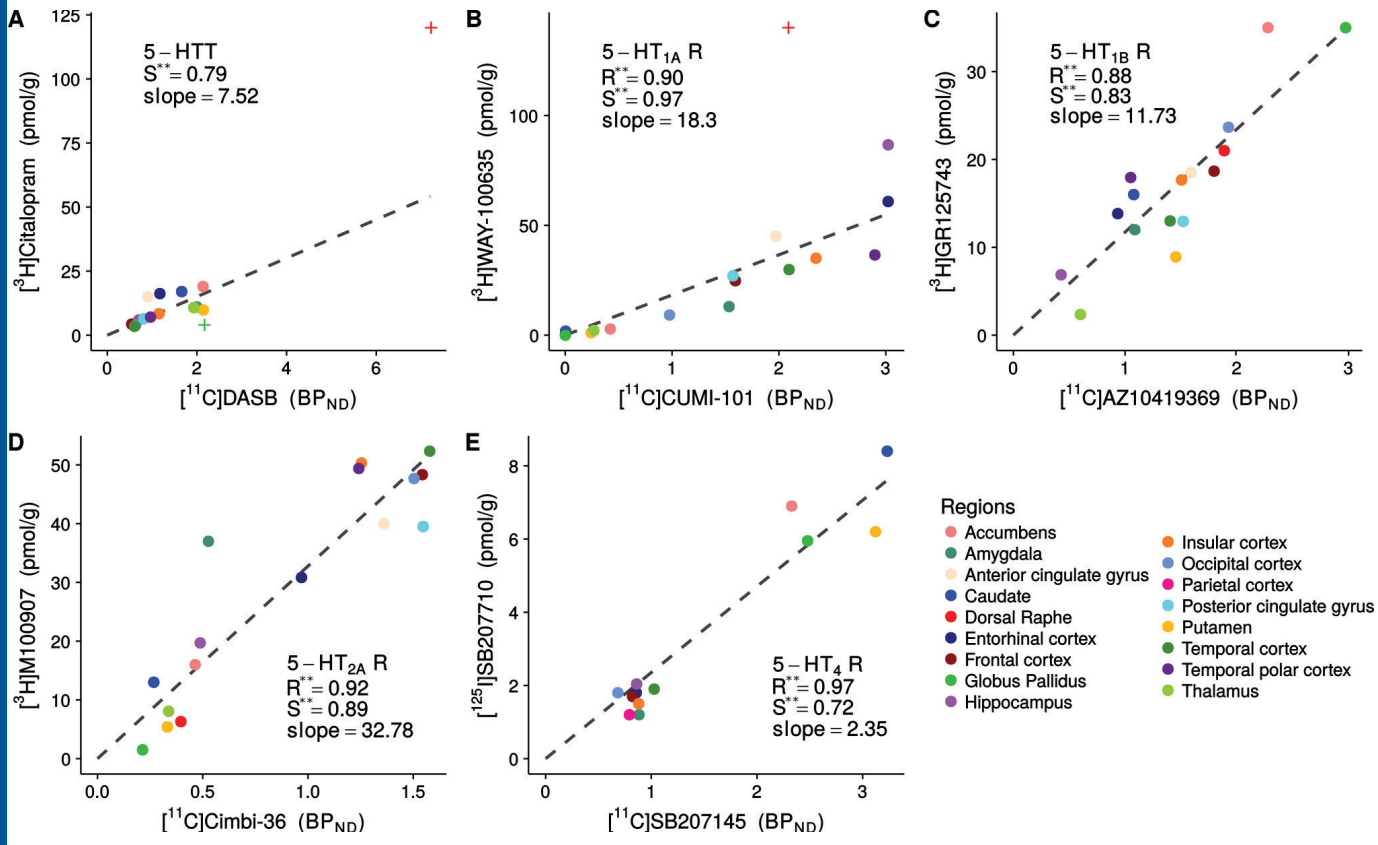

JNeurosci Accepted Manuscript

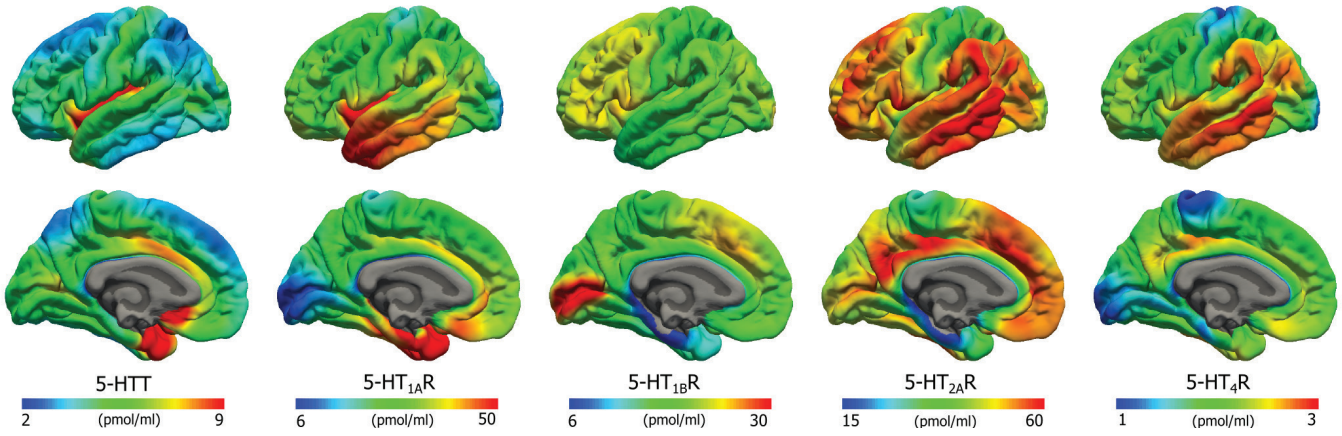

JNeurosci Accepted Manuscript

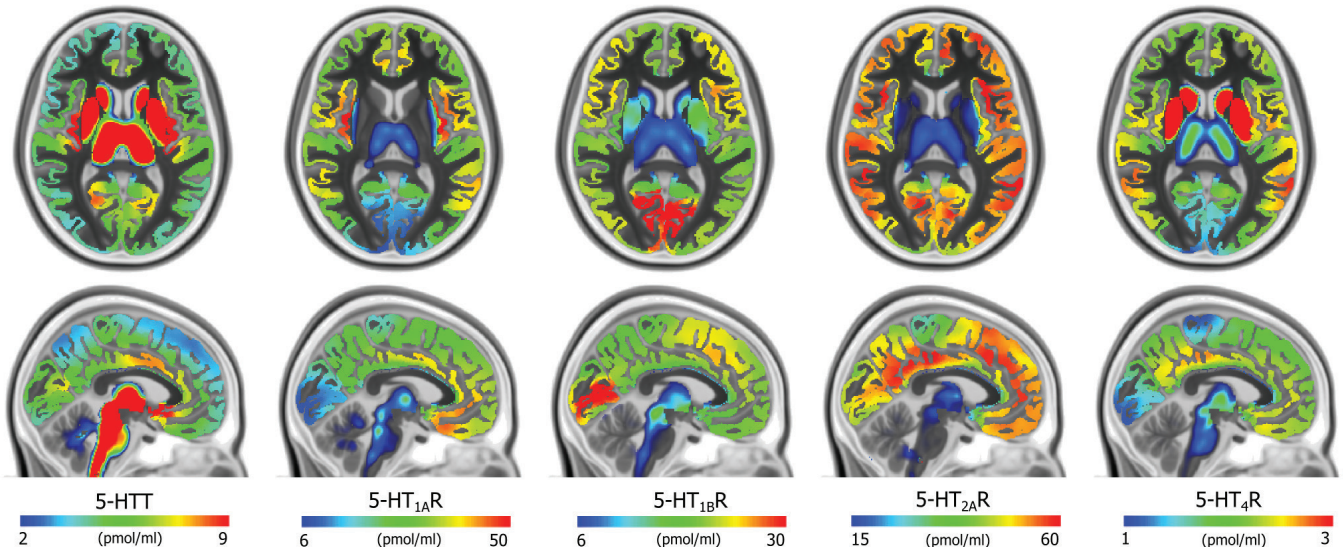

JNeurosci Accepted Manuscript

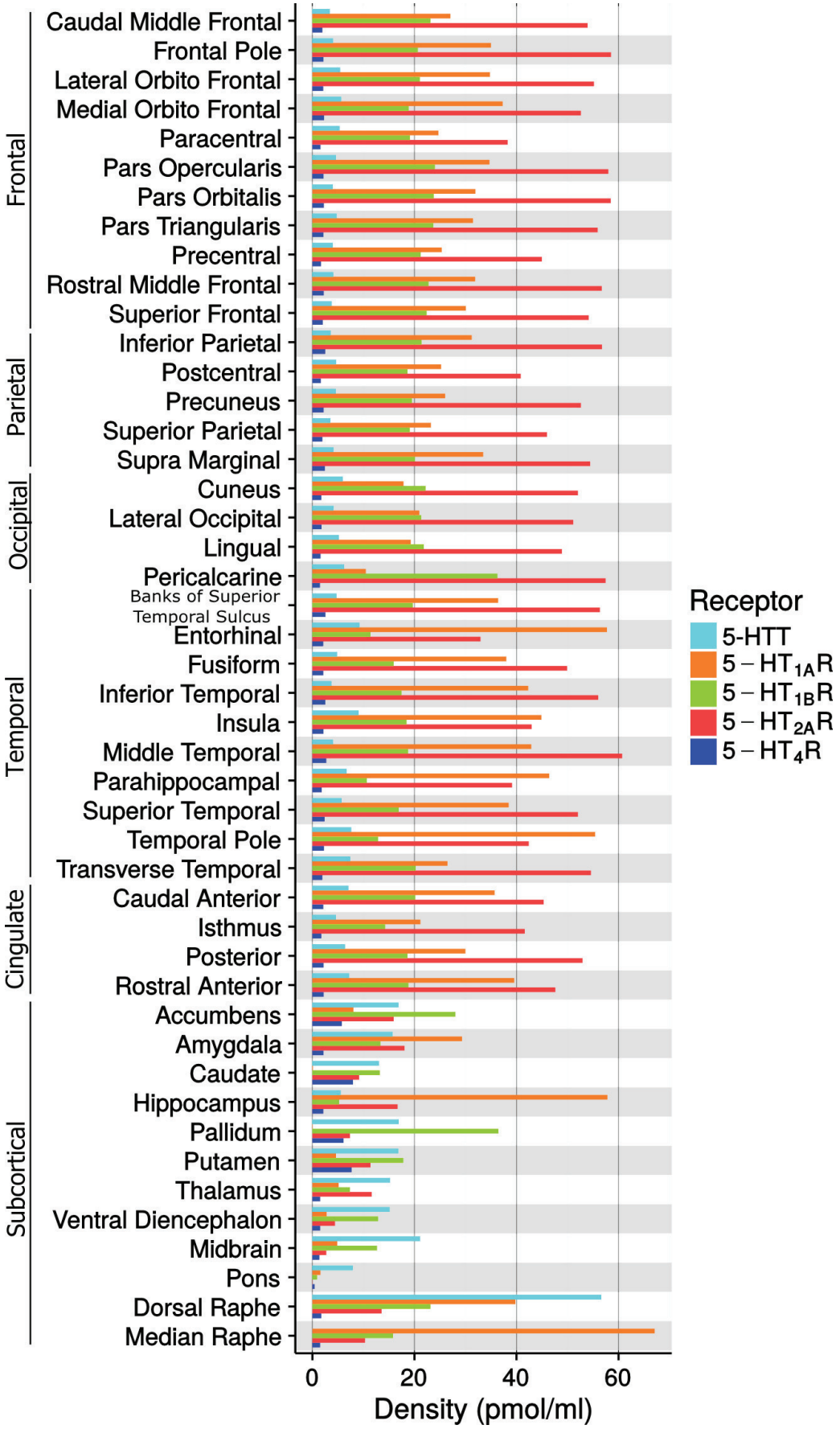

JNeurosci Accepted Manuscript

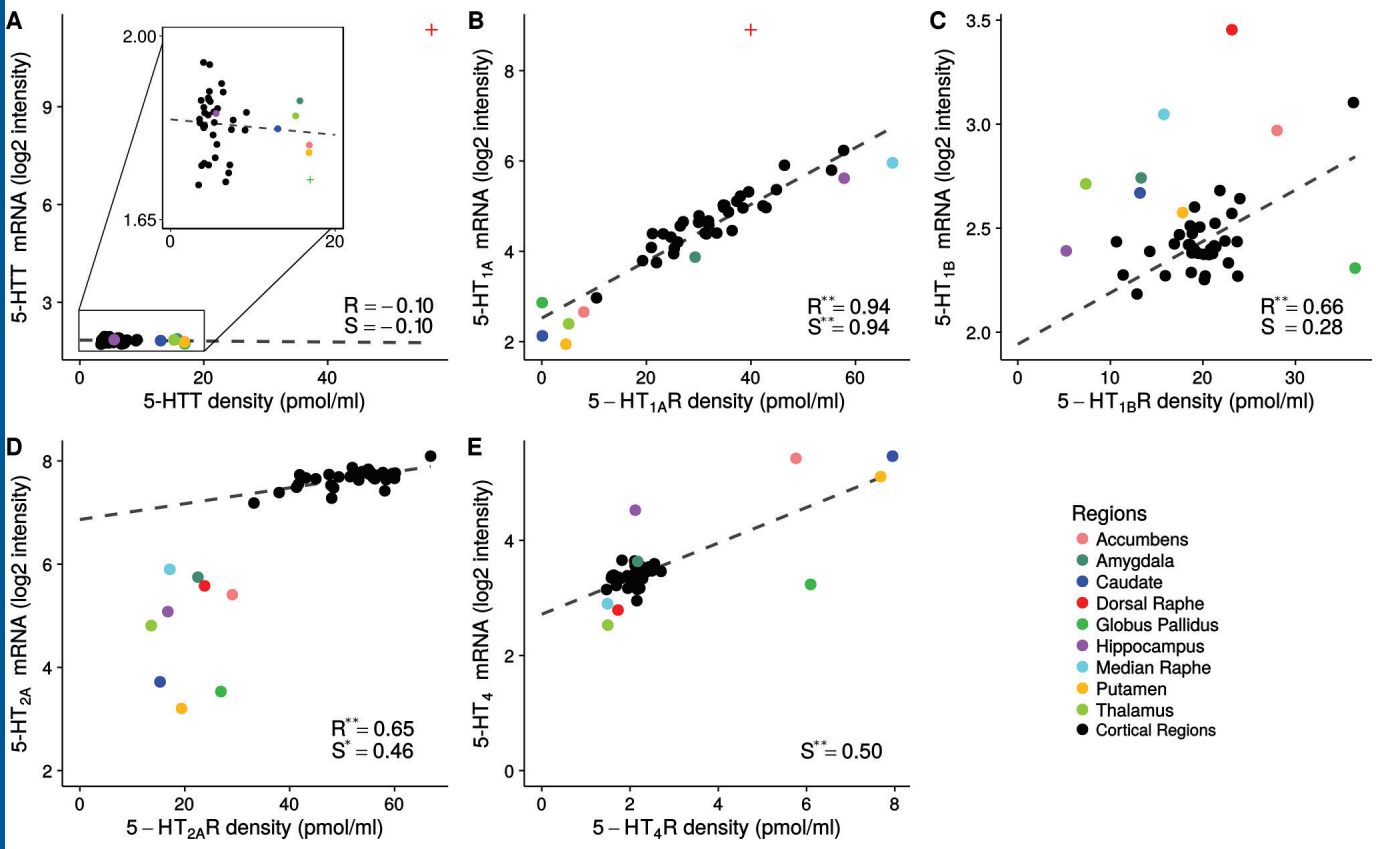
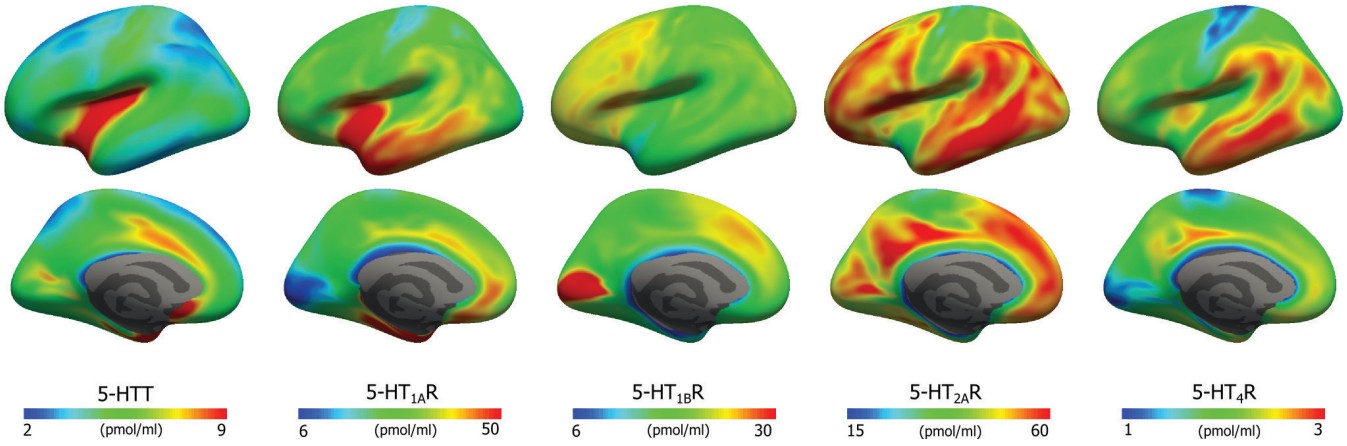
JNeurosci Accepted Manuscript